Nonlinear damping amplifier friction bearings

Sudip Chowdhury[1]
James Watt School of Engineering,
The University of Glasgow,
University Avenue,
Glasgow, G12 8QQ, United Kingdom
email: Sudip.Chowdhury@glasgow.ac.uk

Sondipon Adhikari
James Watt School of Engineering,
The University of Glasgow,
University Avenue,
Glasgow, G12 8QQ, United Kingdom
email: Sondipon.Adhikari@glasgow.ac.uk

The paper introduces damping amplifiers integrated into the core material of conventional nonlinear friction base isolators to improve their vibration attenuation capabilities and mitigate their shortcomings. Four new types of damping amplifier friction bearings are introduced: levered, nested, compound, and damping. The H_2 optimisation strategy is utilised to obtain the closed-form analytical solution for the optimised designed parameters. The analytical investigation confirms the efficiency of the recently obtained closed-form equations for the optimal design parameters. The frequency response function was used to develop closed-form formulas for the isolator and main structure's dynamic responses. The harmonic and random white-noise excitation served as the basis. Furthermore, numerical analysis by considering real earthquake load has confirmed the novel isolators' efficiency. The vibration reduction capacities of the H_2 optimised damping amplifier friction bearings, compound damping amplifier friction bearings, nested damping amplifier friction bearings, and levered damping amplifier friction bearings are 76.1 % superior to the optimum conventional base isolator. These findings demonstrate how the proposed designs may improve structural resistance to dynamic loads.

Keywords: Damping amplifier friction bearing, Compound damping amplifier friction bearing, Nested damping amplifier friction bearing, Levered damping amplifier friction bearing, H_2 optimisation strategy.

1 Introduction

In earthquake engineering, base isolation is a strategy for protecting structures from seismic forces. The purpose of base isolation is to isolate an earthquake's ground motion from a building or other structure [1]. It reduces the impact of seismic pressures on the structure in this manner. Base isolators insulate the building's base from the foundation. These isolators can be made from a variety of materials, including rubber bearings, friction bearings, ball bearings, and spring systems [2]. They allow the building to move independently of the motion of the earth. During an earthquake, the ground trembles, but the building that is insulated from the base remains relatively stable. The isolators absorb and diffuse seismic energy, avoiding its direct transfer to the superstructure. The building is thus subjected to significantly decreased forces and accelerations [3]. Improved seismic performance: Base separation increases a structure's earthquake resilience. Maintaining the building's integrity: It protects it from damage. Retrofitting: Base isolation can be used to improve the seismic resistance of an existing structure [4]. Base isolation systems have been implemented in significant monuments such as City Halls in Pasadena, San Francisco, and Los Angeles. On a smaller scale, base isolation is used to protect vital equipment in isolated raised-floor systems. Although base isolation is not completely earthquake-resistant, it significantly improves a building's chances of survival [5].

There are several potential drawbacks to base isolation, a seismic protection technology that reduces the impact of ground shaking on structures: Rubber used in isolators may degrade over time and require replacement or repair. Base isolation is effective in some building types, such as low- to mid-rise buildings [6]. It may not be suitable for excessively tall or asymmetrical buildings. Retrofitting base isolation into older buildings can be challenging and costly, often requiring significant structural adjustments. Base isolation systems require space to move horizontally and vertically, which may not be practicable in crowded areas or in constructions with low ceiling heights [7]. Base isolation works well in mild earthquakes, but it may not perform as well in really large ones. If ground motion exceeds design limitations, isolators may be overloaded. Base isolators may not protect against other types of loads, such as wind or blast loads, and are primarily designed to withstand seismic stress. It may be challenging to guarantee that base isolation is compatible with current utilities (such as plumbing and electrical systems), as these services must allow for the mobility of the isolated structure [8]. Inconsistencies and uncertainty in design may come from the absence of defined codes and rules for base isolation system design and implementation [9].

Overcoming the problems of base isolation requires a combination of technological advancements, regulatory development, and strategic planning. Here are a few solutions to handle these issues:

(1) Invest in research to develop materials that are resistant to environmental degradation and need fewer replacements over time.
(2) Provide specific isolation solutions for a variety of building types, including taller or asymmetrically constructed structures [10].
(3) Provide modular base isolation systems that can be easily modified for retrofitting existing structures.
(4) Create fundamental isolation systems, including compact or low-profile isolators, that take up less space while maintaining performance.
(5) Using sophisticated seismic modeling and simulation technology can help you forecast and plan for extreme occurrences more accurately.
(6) To enhance overall performance, combine base isolation with other earthquake protection technologies like bracing systems or dampers [11].
(7) Provide adjustable utility and service connections so that base-isolated structures can move around.
(8) Over-increased static mass of the dampers. Adaptability of the bearings when the ground motion load pattern changes from far-field to near-field.
(9) Include architectural features such as damping systems to reduce swaying and restrict the building's movement [12] during seismic events.
(10) The dynamic response reduction capacity of bearings is comparatively lower in high-rise buildings than in single

[1]Corresponding Author.
Version 1.18, August 29, 2025

or low-storey buildings.

(11) Lack of optimal design parameters in terms of exact closed-form expressions. The optimal design parameters will provide more feasibility to the bearings and the robust vibration reduction capacity can be achieved from the optimum bearings.

Although base isolation methods have potential, they include inherent limitations. Challenges include compatibility with elevated or irregular structures, material deterioration over time, and the complexities of retrofitting into pre-existing buildings. Moreover, conventional designs often lack appropriate settings to enhance performance during random seismic excitation. These deficiencies need novel solutions to improve structural robustness. In fact, the majority of the limitations have been solved by offering analytical closed-form expressions for optimal design parameters to the bearings while designing them for the structures [13]. The H_2 optimisation approach has been used to resolve these concerns. In addition, the closed-form expressions for the optimal design parameters have been achieved using the H_2 optimisation method. This approach seeks to reduce the mean-square response of a base-isolated structure subjected to stochastic seismic disturbances. The H_2 technique yields closed-form equations for optimum design parameters by developing frequency response functions and addressing stochastic optimisation concerns, so assuring less vibration and improved isolation efficiency. This method underpins the analytical work detailed in this paper. The H_2 optimisation technique for base isolation requires stochastic analysis to account for random excitation, such as seismic ground motions are considered in random processes. This implies considering the statistical properties of both the responses and the stimulation [14]. Here is a detailed explanation of how base isolation under random stimulation is maximised using H_2. The objective is to lower a base-isolated structure's mean-square reactivity, or energy, to random seismic excitations. Create frequency response functions using random excitation to depict the structure and base isolation system [15]. Solve the H_2 optimisation problem using stochastic processes. To verify robustness, use frequency-domain analysis and stochastic simulations to evaluate performance. Compared to non-optimised systems, optimised systems have lower peak and root-mean-square (RMS) responses [16].

Currently, inerters are integrated into or alongside conventional base isolation systems to augment energy dissipation by increasing the effective mass via rotating mass with motion transformers included in the system. The inerter was first shown by Smith [17] to diminish the efficacy of the existing analogy for mitigation about the vibration responses of the constructions in 2002. Lever mechanisms, which enhance the displacements and velocities impacting the damping device, may be used to address the shortcomings of the existing isolators. A displacement amplification device (DAD) using a gear-type mechanism, which is serially coupled to a fluid viscous damper (FVD), is applied in the conventional base isolators to enhance their seismic performances [18]. Non-linear viscous fluid dampers (NLDs) are sophisticated energy dissipation devices that use fluid dynamics to reduce vibrations in structures. These dampers demonstrate a non-linear response defined by two separate phases: a sticking phase at low displacements dominated by static friction, and a sliding phase at elevated displacements when considerable energy dissipation transpires. Nonlinear dampers (NLDs) excel in handling dynamic loads due to their non-linear characteristics, enabling adaptive performance, which makes them ideal for applications necessitating excellent vibration control under fluctuating load circumstances [19]. Most of the inerter-based and displacement isolation devices are made of flywheel-gear and fluid dynamics mechanisms which do not have the potential to mitigate the existing drawbacks of the conventional base isolators. Therefore, an alternate device is needed that can amplify the effective system parameters of the isolators during vibrations and simultaneously overcome the drawbacks of the dampers. Inertial amplifiers, also known as mass amplification devices, increase forces or movements by utilising their inertial properties [20]. This approach often entails amplifying small input forces or displacements into much larger, useful outputs by the deliberate application of mechanical leverage, resonance, or inertial effects [21]. Inertial amplifiers use a mass's inertia to amplify minuscule input forces [22]. This is commonly accomplished by mechanical devices that leverage a larger mass's inertia to generate a proportionately stronger force or displacement [23]. These devices are capable of using mechanical leverage, which is a system of levers or gears that converts a little force applied over a short distance into a larger force delivered over a longer distance. Resonance is a strategy where a system is designed to oscillate at a given frequency [24]. When applied at the resonant frequency, modest periodic pressures can cause the system to accumulate larger oscillations, magnifying the input [25]. These instruments help to measure and manage vibrations in structures and machinery, which reduces damage and improves engineering performance. In many scientific and technical applications, inertial amplifiers are crucial mass amplification devices [26]. These devices use resonance, mechanical leverage, and inertia to magnify small inputs into larger, more usable outputs. This enables more precise measurement and control of forces and motion. The negative stiffness devices are integrated into the inertially amplified devices to enhance their seismic performances [27]. The damping of inertially amplified hosting structures can be amplified, resulting in increased vibration attenuation capacity of the amplifier [28]. As a result, the frequency of the inertial amplifiers is altered, and effective damping increases, potentially lowering the production cost of vibration attenuation devices [29]. The use of these amplifiers has also lowered the amount of material required. Nevertheless, damping amplifiers are absent from the existing research overview, underscoring a notable deficiency in the present landscape of seismic isolation technology. Current base isolators, such as friction bearings, rubber bearings, and ball bearings, mostly depend on static mass or linear arrangements, which often restrict their capacity to dynamically adjust to fluctuating excitation circumstances, including near-fault and far-field earthquakes. Moreover, several designs encounter obstacles like material deterioration, restricted application to asymmetrical buildings, and insufficient performance under strong earthquake forces. The lack of flexible mechanisms in these isolators has limited their ability to meet the changing requirements of seismic resilience efficiently. Moreover, despite progress in inertial amplification mechanisms and damping systems, previous research has not investigated the incorporation of damping amplifiers directly into the core material of friction base isolators. This mechanism can enhance the effective damping without adding additional materials to the bearings. Furthermore, damping amplifier friction bearings and their optimal design parameters do not exist in the current state of the art.

The paper introduces damping amplifiers integrated into the core material of conventional nonlinear friction base isolators to improve their vibration attenuation efficacy and rectify intrinsic deficiencies. The proposed technology integrates damping amplifiers into the core material via the use of rhombus-type arrangements inside the isolators. These arrangements provide inertial forces that alter the effective damping of the isolators during vibration. The inertial amplification mechanism enhances the damping effect using mechanical configurations, including nested or levered designs, inside the isolator's construction. This integration improves vibration damping by dynamically modifying the isolator's response according to the applied stimulation. Four types of damping amplifier friction bearings are introduced: damping, compound, nested, and levered. The H_2 optimisation approach is used to generate the closed-form analytical solution for the optimum designed parameters. The analytical analysis validates the efficiency of the newly obtained closed-form equations for optimal design parameters. The frequency response function was used to obtain closed-form formulas for the dynamic responses of the main structure and isolator. The harmonic and random excitations were used as base excitations. Further, the analytical investigations and the simulation works are validated by a numerical study by considering

real earthquake load. The innovative isolators' vibration reduction capacity was compared to that of traditional isolators.

2 Damping amplifier friction bearings

The structural diagram of a single-degree-of-freedom system isolated by nonlinear damping amplifier friction bearings subjected to base excitation has been shown in Figure 1. The rectangular

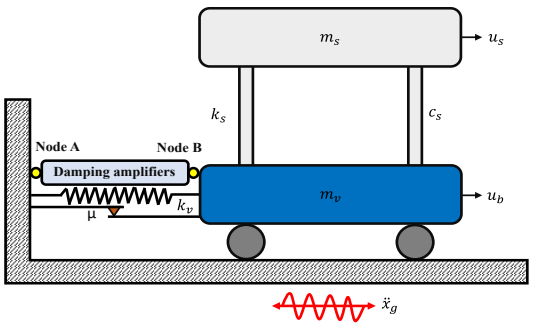

Fig. 1 The structural diagram of a single-degree-of-freedom system isolated by nonlinear damping amplifier friction bearings. The yellow-highlighted circles denote the connecting nodes (Node A and Node B) via which the damping amplifiers are incorporated.

shape diagram with two nodes, such as Node A and Node B in Figure 1 illustrates the conceptual design of the damping amplifier component in each innovative damping amplifier friction bearing. m_s, k_s, and c_s define the mass, stiffness, and damping of the single-degree-of-freedom system. m_v and k_v define the mass and stiffness of the bearings. μ defines the coefficient of friction. Gravity's acceleration is defined as g. $\ddot{x}_g$ defines the base excitation. u_s and u_b define the absolute deflections of the SDOF systems and the bearings. The structural diagrams of each novel friction bearing, such as damping amplifier friction bearing, compound damping amplifier friction bearing, nested damping amplifier friction bearing, and levered damping amplifier friction bearing, are shown in Figure 2. Newton's second law was used to establish the

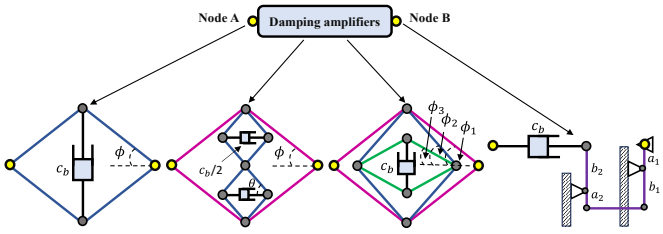

Fig. 2 The structural diagrams of damping amplifier friction bearing, compound damping amplifier friction bearing, nested damping amplifier friction bearing, and levered damping amplifier friction bearing. The yellow-highlighted circles denote the connecting nodes (Node A and Node B) via which the damping amplifiers are incorporated. The blue, pink, green, and purple lines denote the rigid links inside the isolator structures.

governing equations of motion for each isolated single-degree-of-freedom system. The governing equation of motion for the isolated single-degree-of-freedom system was derived as

$$m_s\ddot{x}_s + m_s\ddot{x}_b + c_s\dot{x}_s + k_s x_s = -m_s\ddot{x}_g \tag{1}$$

The governing equation of motion of the novel isolator has been derived as

$$m_v\ddot{x}_b + c_v\dot{x}_b + k_v x_b + \mu\, m_v\, g\, \mathrm{sgn}\,(\dot{x}_b) - c_s\dot{x}_s - k_s x_s = -m_v\ddot{x}_g \tag{2}$$

The relative deflection of single-degree-of-freedom systems and isolators is defined as $x_s = u_s - u_b$ and $x_b = u_b - x_g$, respectively. x_g defines the base deflection. An inertial force is generated inside the damping amplifier due to the application of vibration on the isolated structure. Accordingly, the static damping of the isolators is changed due to their rhombus-type diagrams. After considering the inertial forces generated inside the rhombus, the effective damping of the isolators is derived as

Damping amplifier friction bearing (DAFB)

Effective damping c_v: $c_b \underbrace{\cot^2\phi}_{\Phi}$, where c_b defines the static damping of the DAFB. ϕ defines the amplifier angle.

Compound damping amplifier friction bearing (CDAFB)

Effective damping c_v: $c_b \underbrace{\cot^2\phi\left(\frac{\tan^2\theta}{4}\right)}_{\Phi}$, where c_b defines the static damping of the CDAFB. ϕ and θ define the primary and secondary amplifier angles.

Nested damping amplifier friction bearing (NDAFB)

Effective damping c_v: $c_b \underbrace{\cot^2\phi_1 \tan^2\phi_2 \cot^2\phi_3}_{\Phi}$, where c_b defines the static damping of the NDAFB. ϕ_1, ϕ_2, and ϕ_3 define the primary, secondary, and tertiary amplifier angles.

Levered damping amplifier friction bearing (LDAFB)

Effective damping c_v: $c_b \underbrace{\left(\frac{b_1}{a_1}\frac{b_2}{a_2}\right)^2}_{\Phi}$, where c_b defines the static damping of the LDAFB. $\left(\frac{b_1}{a_1}\frac{b_2}{a_2}\right)$ defines the lever arm ratios.

Overall, Φ defines the damping amplification factor for each novel friction bearing.

To use the H_2 optimisation strategy, each nonlinear element of the governing equation of motion is linearised using the statistical linearization method on Eq. (2). When considering the nonlinear hysteretic response of the isolated structure, the H_2 optimisation approach is used to determine the exact closed-form expressions of the optimal design parameters of the isolators and to provide an appropriate tuning of natural frequency to the isolated structures. The isolators' equivalent damping can be calculated as

$$c_e = E\left\{\frac{\partial\left(\mu m_v g \mathrm{sgn}(\dot{x}_b)\right)}{\partial\dot{x}_b}\right\} = \sqrt{\frac{2}{\pi}}\frac{\mu m_v g}{\sigma_{\dot{x}_b}} \tag{3}$$

$\sigma_{\dot{x}_b}$ defines the square root of the standard deviation of the velocity response of the bearings. Equation (3) has been substituted in Eq. (2). Accordingly, the governing equation of motion of the novel isolator has been derived as

$$m_v\ddot{x}_b + \underbrace{(c_v + c_e)}_{c_{ev}}\dot{x}_b + k_v x_b - c_s\dot{x}_s - k_s x_s = -m_v\ddot{x}_g \tag{4}$$

where x_g defines the base displacement. The steady state solutions are considered: $x_b = X_b e^{i\omega t}$, $x_s = X_s e^{i\omega t}$, and $\ddot{x}_g = X_g e^{i\omega t}$. These solutions are substituted in Eq. (1) and Eq. (4). As a result, a transfer function has been derived using the Laplace transformation [30] and expressed as

$$\begin{bmatrix} 2\mu_v\xi_v\omega_v q\Phi + \mu_v q^2 + \mu_v\omega_v^2 & -2\xi_s\omega_s q - \omega_s^2 \\ q^2 & 2\xi_s\omega_s q + q^2 + \omega_s^2 \end{bmatrix}\begin{Bmatrix} X_b \\ X_s \end{Bmatrix} = -\begin{bmatrix} \mu_v \\ 1 \end{bmatrix} X_g \tag{5}$$

where $q = \mathrm{i}\omega$. i defines the imaginary number and ω defines the angular frequency of excitation. $\mu_v = m_v/m_s$, ω_v, and ξ_v define the mass ratio, natural frequency, and damping ratio of the bearings. ω_s and ξ_s define the natural frequency and damping ratio of the SDOF system. The transfer function of the displacement of the SDOF system is obtained as

$$W_s(\mathrm{i}\omega) = \left.\frac{X_s}{X_g}\right|_{q=\mathrm{i}\omega} = \frac{-\left(2\Phi q\xi_v + \omega_v\right)\mu_v\omega_v}{\delta_f} \tag{6}$$

The transfer function of the displacement of the isolator is obtained as

$$W_b(\mathrm{i}\omega) = \left.\frac{X_b}{X_g}\right|_{q=\mathrm{i}\omega} = \frac{-2\mu_v q\xi_s\omega_s - \mu_v q^2 - \mu_v\omega_s^2 - 2\xi_s\omega_s q - \omega_s^2}{\delta_f} \tag{7}$$

The denominator of Eq. (6) and Eq. (7) has been obtained as

$$\begin{aligned}\delta_f = {} & \mu_v q^4 + \left(2\Phi\mu_v\xi_v\omega_v + 2\xi_s\omega_s\mu_v + 2\xi_s\omega_s\right)q^3 \\ & + \left(4\Phi\mu_v\xi_s\xi_v\omega_s\omega_v + \mu_v\omega_s^2 + \mu_v\omega_v^2 + \omega_s^2\right)q^2 \\ & + \left(2\Phi\mu_v\xi_v\omega_s^2\omega_v + 2\mu_v\xi_s\omega_s\omega_v^2\right)q + \mu_v\omega_s^2\omega_v^2\end{aligned} \tag{8}$$

The isolated SDOF system is subjected to random white excitation. H_2 optimisation is applicable, and the standard deviation of the displacement of the SDOF system is derived using Eq. (6) and Eq. (8).

Derivation of the optimal design parameters by considering $\xi_s \neq 0$

The damping of the main structure is not considered zero for this study, i.e., $\xi_s \neq 0$. Equation (8) is a fourth-order polynomial equation, and applying the H_2 optimisation method for random white noise excitation, the standard deviation for the displacement of the SDOF system [14] is derived as

$$\sigma_{w_s}^2 = \frac{S_0\pi\omega_v\begin{pmatrix}4\Phi^3\mu_v^2\xi_s^3\omega_s^2\omega_v + 4\Phi^2\mu_v^2\xi_s\xi_v^2\omega_s^3 \\ +4\Phi^2\mu_v^2\xi_s\xi_v^2\omega_s\omega_v^2 + 4\Phi^2\mu_v\xi_s\xi_v^2\omega_s^3 \\ +4\Phi\,\mu_v^2\xi_s^2\xi_v\omega_s^2\omega_v + 4\Phi\mu_v\xi_s^2\xi_v\omega_s^2\omega_v \\ +\Phi\,\mu_v^2\xi_v\omega_v^3 + \Phi\mu_v\xi_v\omega_s^2\omega_v + \mu_v^2\xi_s\omega_s^3 \\ +2\mu_v\xi_s\omega_s^3 + \mu_v\xi_s\omega_s\omega_v^2 + \xi_s\omega_s^3\end{pmatrix}}{2\omega_s^3\begin{pmatrix}4\Phi^3\mu_v^2\xi_s\xi_v^3\omega_s^2\omega_v^2 + 4\Phi^2\mu_v^2\xi_s^2\xi_v^2\omega_s^3\omega_v \\ +4\Phi^2\mu_v^2\xi_s^2\xi_v^2\omega_s\omega_v^3 + 4\Phi^2\mu_v\xi_s^2\xi_v^2\omega_s^3\omega_v \\ +4\Phi\,\mu_v^2\xi_s^3\xi_v\omega_s^2\omega_v^2 + 4\Phi\mu_v\xi_s^3\xi_v\omega_s^2\omega_v^2 \\ +\Phi^2\mu_v\xi_v^2\omega_s^3\omega_v + \Phi\,\mu_v^2\xi_s\xi_v\omega_s^4 \\ -2\Phi\,\mu_v^2\xi_s\xi_v\omega_s^2\omega_v^2 + \Phi\,\mu_v^2\xi_s\xi_v\omega_v^4 \\ +2\Phi\mu_v\xi_s\xi_v\omega_s^4 + \Phi\xi_s\xi_v\omega_s^4 + \mu_v\xi_s^2\omega_s\omega_v^3\end{pmatrix}} \tag{9}$$

Equation (9) is partially substituted by ξ_v and ω_v to derive their optimal values in terms of closed-form expressions, and the mathematical expressions are derived as

$$\frac{\partial\sigma_{w_s}^2}{\partial\xi_v} = 0 \quad \text{and} \quad \frac{\partial\sigma_{w_s}^2}{\partial\omega_v} = 0 \tag{10}$$

Equation (9) is substituted in the first expression of Eq. (10), and the closed-form expression for the damping ratio of the novel bearings is derived as

$$\xi_v = \frac{\xi_s\left(\mu_v^2\omega_s^2 - 2\mu_v^2\omega_v^2 + 2\mu_v\omega_s^2 - \mu_v\omega_v^2 + \omega_s^2\right)}{2\Phi\mu_v\omega_s\omega_v} \tag{11}$$

Equation (11) is substituted in Eq. (9), and the modified version of Eq. (9) is derived, which contains the optimal frequency of the bearings.

$$\sigma_{w_s}^2 = \frac{S_0\pi\begin{pmatrix}32\mu_v^6\xi_s^2\omega_s^6 - 192\mu_v^6\xi_s^2\omega_s^4\omega_v^2 + 384\mu_v^6\xi_s^2\omega_s^2\omega_v^4 \\ -256\mu_v^6\xi_s^2\omega_v^6 + 208\mu_v^5\xi_s^2\omega_s^6 - 912\mu_v^5\xi_s^2\omega_s^4\omega_v^2 \\ +1152\mu_v^5\xi_s^2\omega_s^2\omega_v^4 - 320\mu_v^5\xi_s^2\omega_v^6 + 560\mu_v^4\xi_s^2\omega_s^6 \\ -1688\mu_v^4\xi_s^2\omega_s^4\omega_v^2 + 1200\mu_v^4\xi_s^2\omega_s^2\omega_v^4 - 128\mu_v^4\xi_s^2\omega_v^6 \\ +800\mu_v^3\xi_s^2\omega_s^6 - 1512\mu_v^3\xi_s^2\omega_s^4\omega_v^2 + 504\mu_v^3\xi_s^2\omega_s^2\omega_v^4 \\ -16\mu_v^3\xi_s^2\omega_v^6 + 2\mu_v^4\omega_s^2\omega_v^4 - 4\mu_v^4\omega_v^6 + 640\mu_v^2\xi_s^2\omega_s^6 \\ -648\mu_v^2\xi_s^2\omega_s^4\omega_v^2 + 72\mu_v^2\xi_s^2\omega_s^2\omega_v^4 + 3\mu_v^3\omega_s^4\omega_v^2 \\ -2\mu_v^3\omega_v^6 + 272\mu_v\xi_s^2\omega_s^6 - 104\mu_v\xi_s^2\omega_s^4\omega_v^2 \\ +6\mu_v^2\omega_s^4\omega_v^2 + \mu_v^2\omega_s^2\omega_v^4 + 48\xi_s^2\omega_s^6 + 3\mu_v\omega_s^4\omega_v^2\end{pmatrix}}{2\begin{pmatrix}32\mu_v^6\xi_s^2\omega_s^6 - 192\mu_v^6\xi_s^2\omega_s^4\omega_v^2 + 384\mu_v^6\xi_s^2\omega_s^2\omega_v^4 \\ +208\mu_v^5\xi_s^2\omega_s^6 - 912\mu_v^5\xi_s^2\omega_s^4\omega_v^2 + 1152\mu_v^5\xi_s^2\omega_s^2\omega_v^4 \\ -320\mu_v^5\xi_s^2\omega_v^6 + 560\mu_v^4\xi_s^2\omega_s^6 - 1688\mu_v^4\xi_s^2\omega_s^4\omega_v^2 \\ +1200\mu_v^4\xi_s^2\omega_s^2\omega_v^4 - 128\mu_v^4\xi_s^2\omega_v^6 + 800\mu_v^3\xi_s^2\omega_s^6 \\ -256\mu_v^6\xi_s^2\omega_v^6 - 1512\mu_v^3\xi_s^2\omega_s^4\omega_v^2 + 504\mu_v^3\xi_s^2\omega_s^2\omega_v^4 \\ -16\mu_v^3\xi_s^2\omega_v^6 + 6\mu_v^4\omega_s^6 - 24\mu_v^4\omega_s^4\omega_v^2 + 26\mu_v^4\omega_s^2\omega_v^4 \\ +640\mu_v^2\xi_s^2\omega_s^6 - 648\mu_v^2\xi_s^2\omega_s^4\omega_v^2 + 72\mu_v^2\xi_s^2\omega_s^2\omega_v^4 \\ -58\mu_v^3\omega_s^4\omega_v^2 + 24\mu_v^3\omega_s^2\omega_v^4 - 2\mu_v^3\omega_v^6 - 4\mu_v^4\omega_v^6 \\ +272\mu_v\xi_s^2\omega_s^6 - 104\mu_v\xi_s^2\omega_s^4\omega_v^2 - 44\mu_v^2\omega_s^4\omega_v^2 \\ +7\mu_v^2\omega_s^2\omega_v^4 + 48\xi_s^2\omega_s^6 + 24\mu_v\omega_s^6 - 10\mu_v\omega_s^4\omega_v^2 \\ +6\omega_s^6 + 24\mu_v^3\omega_s^6 + 36\mu_v^2\omega_s^6\end{pmatrix}\omega_s^3\xi_s} \tag{12}$$

Equation (12) is substituted in the second expression of Eq. (10), and the optimal natural frequency of the isolator is derived as

$$(\omega_v)_{\text{opt}} = \sqrt{\frac{\omega_s^2\left(\mu_v+1\right)^2\left(24\mu_v+13\right)}{12\left(2\mu_v+1\right)^2\mu_v}} \tag{13}$$

Equation (13) is substituted in Eq. (11) to derive the optimal damping ratio of the isolator.

$$(\xi_v)_{\text{opt}} = \frac{\xi_s\left(\mu_v+1\right)^2\sqrt{3}}{24\sqrt{\frac{\left(\mu_v+1\right)^2\left(24\mu_v+13\right)}{\left(2\mu_v+1\right)^2\mu_v}}\,\mu_v\left(\mu_v+\frac{1}{2}\right)\Phi} \tag{14}$$

The standard deviation of the velocity response of the bearings has been derived as

$$\sigma_{\dot{x}_b}^2 = \frac{S_0\pi\,\omega_s^4\left(\mu_v+1\right)^2\left(\Phi\xi_v\omega_s + \xi_s\omega_v\right)}{\begin{pmatrix}8\omega_v^2\mu_v^2\xi_s\Phi^3\xi_v^3\omega_s^2 + 8\Phi^2\mu_v^2\xi_s^2\omega_v\omega_s^3\xi_s^2 + 8\mu_v^2\xi_s^2\omega_s^3\omega_s\Phi^2\xi_v^2 \\ +8\Phi^2\mu_v\xi_v^2\omega_v\omega_s^3\xi_s^2 + 8\omega_v^2\mu_v^2\xi_s^3\Phi\xi_v\omega_s^2 + 8\omega_v^2\mu_v\xi_s^3\Phi\xi_v\omega_s^2 \\ +2\Phi^2\mu_v\xi_v^2\omega_v\omega_s^3 + 2\Phi\,\mu_v^2\xi_s\xi_v\omega_s^4 - 4\omega_v^2\mu_v^2\xi_s\Phi\xi_v\omega_s^2 \\ +2\Phi\,\mu_v^2\xi_s\xi_v\omega_v^4 + 4\Phi\mu_v\xi_s\xi_v\omega_s^4 + 2\Phi\xi_s\xi_v\omega_s^4 + 2\mu_v\xi_s^2\omega_v^3\omega_s\end{pmatrix}} \tag{15}$$

Derivation of the optimal design parameters by considering $\xi_s = 0$

Now, the damping of the main structure is considered zero, i.e., $\xi_s = 0$. Simultaneously, the closed-form expressions for the standard deviation and optimal design parameters for the isolated structure and bearings have been changed. The dynamic effect of the structural damping in the closed-form expressions of the bearing has been excluded. Therefore, in order to obtain the newly derived standard deviation from this analysis, the values of ξ_s in Eq. (6) and Eq. (8) are considered zero. The denominator of Eq. (6), i.e. Eq. (8) is a fourth-order polynomial equation, and applying the H_2 optimisation method for random white noise excitation, the standard deviation for the displacement of the SDOF system [14] is derived as

$$\sigma_{w_s}^2 = \frac{S_0\pi\omega_v\left(4\Phi^2\mu_v\xi_v^2\omega_s^2 + \mu_v\omega_v^2 + \omega_s^2\right)}{2\Phi\xi_v\omega_s^6} \tag{16}$$

Equation (16) is partially substituted by ξ_v and ν_d to derive their optimal values in terms of closed-form expressions, and the mathematical expressions are derived as

$$\frac{\partial \sigma_{\ddot{w}_s}^2}{\partial \xi_v} = 0 \quad \text{and} \quad \frac{\partial \sigma_{\ddot{w}_s}^2}{\partial \omega_v} = 0 \tag{17}$$

Equation (16) is substituted in the first expression of Eq. (17), and the closed-form expression for the damping ratio of the novel bearings is derived as

$$\xi_v = \frac{\sqrt{\mu_v \left(\mu_v \omega_v^2 + \omega_s^2\right)}}{2\mu_v \omega_s \Phi} \tag{18}$$

Equation (18) is substituted in Eq. (16), and the modified version of Eq. (16) is derived, which contains the optimal frequency of the bearing.

$$\sigma_{\ddot{w}_s}^2 = \frac{S_0 \pi \omega_v \left(2\mu_v \omega_v^2 + 2\omega_s^2\right) \mu_v}{\sqrt{\mu_v \left(\mu_v \omega_v^2 + \omega_s^2\right)} \omega_s^5} \tag{19}$$

Equation (19) is substituted in the second expression of Eq. (17), and the optimal natural frequency of the isolator is derived as

$$(\omega_v)_{\text{opt}} = \frac{\omega_s}{\sqrt{2\mu_v}} \tag{20}$$

Equation (20) is substituted in Eq. (18) to derive the optimal damping ratio of the isolator.

$$(\xi_v)_{\text{opt}} = \frac{\sqrt{6}\sqrt{\mu_v}}{4\mu_v \Phi} \tag{21}$$

The standard deviation of the velocity response of the bearings has been derived as

$$\sigma_{\dot{x}_b}^2 = \frac{S_0 \pi \left(\mu_v + 1\right)}{2\mu_v \Phi \xi_v \omega_v} \tag{22}$$

The Figure 3 shows how the ideal frequency ratio of isolators varies with the mass ratio. The analysis is conducted under two distinct scenarios:

1. Figure 3 (a) ($\xi_s \neq 0$):
   - The graph indicates a decrease in the optimum frequency ratio when the isolator mass ratio increases.
   - Lower mass ratios result in a higher optimum frequency ratio of around 1.45.
   - As the mass ratio approaches 1.0, the ideal frequency ratio declines to approximately 1.2.
   - A lowered optimum frequency ratio indicates lesser frequency adjustment needs for the isolator. This is beneficial as it indicates that the system attains optimum isolation performance with reduced requirements for the isolator's natural frequency adjustment. This would typically decrease the necessary stiffness of the isolator's spring or the mass of the inertial components, hence enhancing implementation feasibility. However, $1.4 < \eta_v < 1.2$ values of the optimal frequency ratios do not provide a feasible design for the isolator. It will not provide the minimum required flexibility to the isolator base layer during vibration, which is necessary to dissipate additional energies from the isolator.
2. Figure 3 (b) ($\xi_s = 0$):
   - The graph shows a diminishing trend in the optimum frequency ratio when the isolator mass ratio increases, similar to the damping case.
   - The ideal frequency ratio at a lower mass ratio begins around 0.95.
   - As the mass ratio approaches 1.0, the ideal frequency ratio falls to approximately 0.7.
   - The optimal frequency ratio in this context is often less than that in the damped situation. This indicates a significant decrease in frequency, however, accompanied by practical problems. Extremely low-frequency ratios may need disproportionately large masses or extremely flexible springs, potentially complicating the design, material choices, or geographical limitations. However, $0.7 < \eta_v < 0.9$ values show feasible to achieve robust performance compared to $1.4 < \eta_v < 1.2$. This value gives a feasible extended time period to the isolated structure during seismic events.

Here lower values indicates the value of $0.7 < \eta_v < 0.9$ ranges compared to $1.4 < \eta_v < 1.2$. Consequently, while a reduced frequency ratio aids in attaining adequate vibration isolation, extremely low values may provide practical implementation difficulties. A balance must be maintained to guarantee the feasibility of the design parameters. In actual applications, the ideal frequency ratio must be determined by evaluating both theoretical performance and the practical limitations of mass, stiffness, and system size.

Overall, A lower optimum frequency ratio facilitates vibration isolation; nevertheless, extremely low values may hinder practical implementation by necessitating bigger masses or more flexible springs. Therefore, optimum frequency ratios must be chosen with regard to both isolation performance and the practicality of system design. The figures illustrate an inverse correlation between

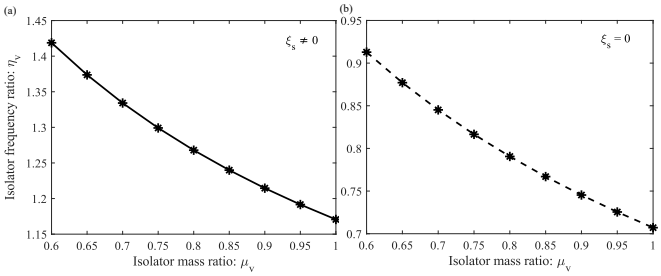

Fig. 3 The variations of optimal frequency ratio of the isolators versus isolator mass ratio after considering (a) $\xi_s \neq 0$, $\xi_s = 0.05$ and (b) $\xi_s = 0$.

the isolator mass ratio and the optimal frequency ratio. The introduction of damping elevates the overall frequency ratios, as seen by the observed trend alterations. Although the overarching pattern (a reduction in the optimal frequency ratio with a rising mass ratio) is consistent across both graphs, the rate of decline or the effects of dampening presence or absence bring minor differences. For example: with structural damping ($\xi_s \neq 0$), the reduction is less significant, resulting in elevated total frequency ratios in comparison to the undamped scenario. In the absence of structural damping ($\xi_s = 0$), the reduction is more pronounced, leading to decreased frequency ratios. Damping helps to manage the frequency response, resulting in a higher ideal frequency ratio than an undamped system. These findings are critical for developing isolation systems because they indicate that the mass ratio and damping properties must be carefully examined in order to obtain optimal vibration isolation performance.

The Figure 4 shows how the ideal damping ratio of isolators varies with the isolator mass ratio in two circumstances. Both

figures look at four types of isolators: damping, compound, nested, and levered.

1. Figure 4 (a) ($\xi_s \neq 0$): The isolator damping ratio varies with the mass ratio.

- Damping isolators: The damping ratio, represented by a dotted blue line, is very low and nearly constant (close to zero) across the mass ratio range.
- Compound isolators: A dashed orange line represents the damping ratio, which is also fairly constant but larger than that of the damping isolators, at roughly 0.5.
- Nested isolators: The damping ratio, represented by a solid yellow line with star markers, is approximately 1.2 higher than that of the damping and compound isolators, with a little diminishing tendency as the mass ratio increases.
- Levered isolators, represented by a solid purple line with star markers, have the largest damping ratios, starting at 3.0×10^{-3} and decreasing slightly as the mass ratio increases.

1. Figure 4 (b) ($\xi_s = 0$): Even without damping, different isolators exhibit distinct patterns in their damping ratios.

- Damping isolators: The damping ratio stays low and practically constant, analogous to the situation of $\xi_s \neq 0$ equals zero or close to it.
- Compound isolators: The damping ratio is pretty stable and slightly above 0.3.
- Nested isolators: The damping ratio is higher, beginning at about 0.5 and progressively falling to about 0.45 as the mass ratio increases.
- Levered isolators: These isolators have the largest damping ratios, which begin at 0.8 and decrease to roughly 0.7 as the mass ratio increases.

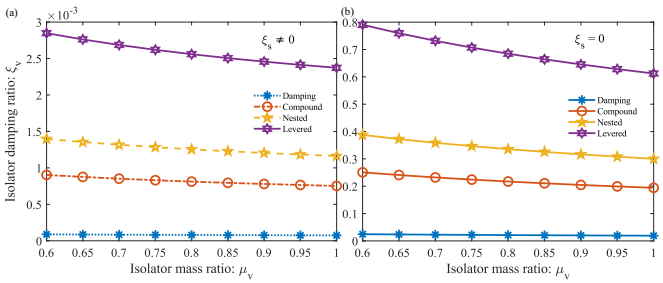

Fig. 4 The variations of optimal damping ratio of the isolators versus isolator mass ratio after considering (a) $\xi_s \neq 0$, $\xi_s = 0.05$ and (b) $\xi_s = 0$.

The damping ratio of a damper can significantly impact production costs. The variations in the damping ratios of the four isolators (damping, compound, nested, and levered) result from their unique structural designs and energy dissipation methods. The Damping Amplifier Friction Bearings (DAFB) has a straightforward design, mostly using frictional damping in the base layer, resulting in a virtually uniform, low damping ratio across the mass ratio spectrum. The Compound Damping Amplifier Friction Bearings (CDAFB) include an angular component (θ) in their design, which improves energy dissipation via an extra amplification mechanism, yielding a somewhat elevated damping ratio compared to DAFB. The Nested Damping Amplifier Friction Bearings (NDAFB) use a stratified arrangement with many rhombus-shaped components. This configuration facilitates a cumulative energy dissipation effect owing to the series arrangement of damping components, markedly enhancing the damping ratio relative to the more basic DAFB and CDAFB. The Levered Damping Amplifier Friction Bearings (LDAFB) use a lever mechanism to efficiently amplify inertial forces, resulting in optimal energy dissipation capacity. This structural advantage renders LDAFB excellent regarding damping ratio performance.

The mass ratio (μ_v) is a crucial determinant of the damping ratio, although several other factors also impact the efficacy of these isolators:

- Geometric configurations: The angular parameters (ϕ, θ, ϕ_1, ϕ_2, ϕ_3) directly affect the effective damping via cotangent and tangent terms in the governing equations for effective damping. The angles dictate the interaction between the isolator structure and the base vibrations, facilitating energy amplification and dissipation.
- Material Properties: The friction coefficient of the isolator materials and the stiffness of the springs used in the isolators influence their damping efficacy.
- Dynamic Characteristics of the Structure: The natural frequency of the main structure (ω_s) and the damping ratio (ξ_s) significantly influence the interaction dynamics between the structure and the isolator.
- Configurations of Isolators: Parameters include the lever arm ratios in LDAFB (a_1/b_1, a_2/b_2) and the mass distribution in nested and compound systems affect the damping ratio.

This research ensured a fair comparison by maintaining uniform material characteristics and structural factors, such as stiffness and friction coefficients, across all isolator types. The angular configurations and mass ratios were selected to remain within feasible design parameters, but the dynamic characteristics of the principal structure were maintained consistently throughout all scenarios. This enabled a fair assessment of the damping ratios and guaranteed that the noted discrepancies were only attributable to the structural mechanisms of the isolators.

The mass ratio (μ_v) is a crucial element affecting the isolator's performance, while the damping ratio dictates energy dissipation. To achieve optimum vibration isolation, the damping ratio must equilibrate energy dissipation with the reduction of energy transmission. An excessively high damping ratio may cause excessive energy dissipation, restricting isolator flexibility, while an excessively low damping ratio may result in insufficient vibration attenuation. A well-tuned damping ratio is essential for attaining the appropriate vibration isolation efficacy. A lower damping ratio (i.e., $0.05 \leq \xi_v \leq 0.8$) is essential for achieving effective vibration reduction since an optimal damping ratio is crucial for balancing energy dissipation and limiting energy transmission through the isolator. A lower damping ratio provides low material and manufacturing costs which is very much essential for a sustainable construction.

The assumption of a mass ratio between 0.6 and 1 is feasible for systems where isolators include substantial inertial elements, such as levers or nested structures, to attain high vibration attenuation efficacy. Although this mass ratio may seem substantial, it is practical in applications such as seismic isolation or the protection of precise instruments. Consolidating the isolator mass into a singular equivalent mass is a legitimate simplification for analytical modeling, especially when the components of the isolator function as an integrated system. The compound damping amplification and other internal processes (e.g., lever systems, nested structures) are included via the generated effective damping and stiffness parameters. These words capture the contributions of internal configurations, ensuring the model accurately reflects physical behavior. This research employs the H_2 optimisation framework to verify the lumped-parameter method by delivering optimum design parameters that correspond effectively with the actual performance of the isolators. Furthermore, the lumped-mass assumption is extensively used in vibration isolation research, offering a compromise between model intricacy and computational efficiency. The

lumped-mass assumption streamlines the modeling process while maintaining precision by including compound damping amplification and other internal processes in the resultant effective damping and stiffness parameters. This methodology guarantees that the model accurately reflects physical behavior while preserving computing efficiency.

3 Dynamic response evaluation

The newly developed damping-amplifier base isolators and tuned mass dampers are applied to single degree of freedom systems to satisfy each of their vibration reduction performance objectives. All regulated single-degree-of-freedom (SDOF) systems share the same governing system parameters. Harmonic excitation is used

Table 1 The structural system parameter for the single degree of freedom system.

Primary structure	Governing system parameter	Value
		ξ_s
SDOF	Damping ratio	0.01

at the base of the controlled structures. As a result, dynamic responses arise from controlled structures. The complete examination of dynamic response evaluation is presented below. The damping ratio of ξ_s =1 % was chosen to represent a lightly damped primary structure, ensuring that the performance of the isolators is evaluated under conservative conditions. While typical building damping ratios range from 2 % to 5 %, this value is realistic for flexible structures or lightly damped systems and allows the isolators' contribution to vibration reduction to be more clearly observed.

3.1 Single degree of freedom systems isolated by the novel base isolators. Each isolator is applied at the base of the single degree of freedom systems subjected to the harmonic base excitation. First, the H_2 optimised base isolators are applied to the single degree of freedom systems to determine their vibration reduction performances. The governing system parameters for the single degree of freedom systems and the H_2 optimised base isolators are listed in Table 1 and Table 2. The optimal displacements of the isolated

Table 2 H_2 optimised design parameters for the conventional and novel base isolators.

System	Introduced by	H_2 optimisation	
		η_d	ξ_d
Damping	This study	0.745356	0.454487
Compound	This study	0.745356	0.432459
Nested	This study	0.745356	0.454487
Levered	This study	0.745356	0.645497
CBI	Matsagar and Jangid [31]	0.50	0.10

Conventional base isolator (CBI): isolator mass ratio (μ_v) = 0.90, DAFB: μ_v = 0.90, $\phi = 40^o$; CDAFB: μ_v = 0.90, $\phi = 40^o$, $\theta = 64^o$; NDAFB: μ_v = 0.90, $\phi_1 = 40^o$, $\phi_2 = 45^o$, $\phi_3 = 45^o$, and LDAFB: μ_v = 0.90, b_1/a_1 = 1.0, b_2/a_2 = 1.0. These parameters are applied to the Eq. (20) and Eq. (21) to obtain each H_2 optimised base isolator's optimal natural frequency and damping ratio.

single-degree-of-freedom systems are derived using these optimal design parameters and the frequency response functions, which are developed in the previous sections. The vibration reduction performance is estimated by comparing it with the optimum conventional base isolators. The governing system parameters for the conventional base isolators are taken from a well-established paper. The paper is cited in Table 2. The mass ratio of the conventional base isolator and the novel base isolators are maintained exactly the same to perform a fair comparison between their vibration reduction performances. Now, after applying all system parameters, the variations in the optimal displacements of the single degree of freedom systems isolated by the H_2 optimised ordinary, compound, nested, and Levered DAFBs as a function of the frequency ratio are obtained and graphically presented in Figure 5. The max-

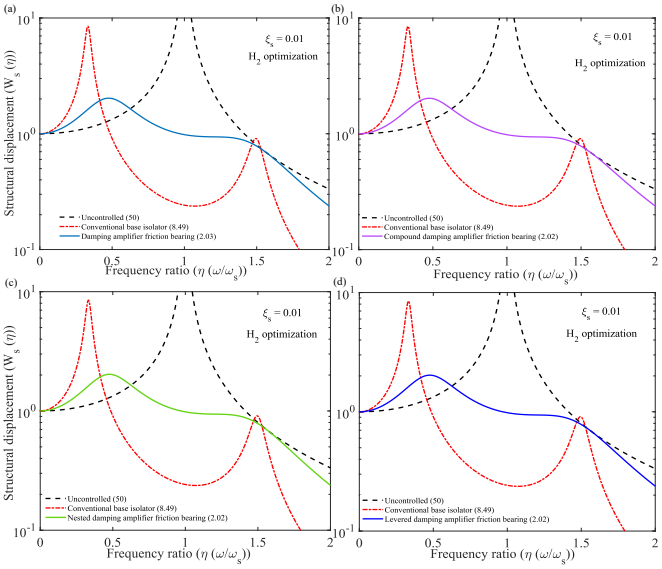

Fig. 5 Variations in the optimal displacements of the single degree of freedom systems isolated by the H_2 optimised (a) ordinary, (b) compound, (c) nested, and (d) Levered DAFBs as a function of the frequency ratio of the harmonic excitation.

imum displacement response of the uncontrolled single degree of freedom system is also obtained analytically using the frequency response function and the value is 50. The maximum displacement responses of the single degree of freedom systems isolated by H_2 optimised ordinary, compound, nested, and Levered DAFBs are obtained as 2.03, 2.20, 2.02, and 2.02. The maximum displacement response of the single degree of freedom system isolated by the conventional base isolator is obtained as 8.49. The vibration reduction capacities of the novel isolators are derived with respect to the conventional base isolator, and the mathematical expression for the required derivation is as follows.

$$W_{\mathrm{dr}}(\%) = \left(\frac{(W_s(\eta))_{\mathrm{conventional}} - (W_s(\eta))_{\mathrm{novel}}}{(W_s(\eta))_{\mathrm{conventional}}} \right) \times 100 \qquad (23)$$

where $(W_s(\eta))_{\mathrm{conventional}}$ and $(W_s(\eta))_{\mathrm{novel}}$ define the maximum displacement of the single degree of freedom system isolated by the conventional and the novel base isolators. The maximum displacement responses of the single degree of freedom systems isolated by H_2 optimised conventional, ordinary, compound, nested, and Levered DAFBs are applied to the Eq. (23). Accordingly, the vibration reduction capacity of the ordinary, compound, nested, and Levered DAFBs is 76.1 % superior to the conventional base isolator.

The approach outlined in this section incorporates a white noise base excitation. Consequently, more experiments are conducted to validate the dependability of the proposed method over a broader range of seismic excitation situations. The Clough-Penzien power spectrum, an adapted variant of the prevalent Kanai-Tajimi spectrum, may be used as the ground acceleration for this investigation to achieve this objective. The unilateral PSD inherent in the process distinguishes it.

$$X_{\ddot{x}_g} = S_0 \frac{\omega_d^4 + 4\zeta_d^2\omega_d^2\omega^2}{\left(\omega_d^2 - \omega^2\right)^2 + 4\zeta_d^2\omega_d^2\omega^2} \frac{\omega^4}{\left(\omega_r^2 - \omega^2\right)^2 + 4\zeta_r^2\omega_r^2\omega^2} \qquad (24)$$

The constant power spectral density for random white noise excitation is denoted by S_0. The renowned Kanai-Tajimi model's filter parameters are ω_d and ζ_d, denoting the natural frequency and damping ratio of the soil layer, respectively. The variations in the optimal displacements of the single degree of freedom systems isolated by the H_2 optimised ordinary, compound, nested, and Levered DAFBs as a function of the frequency ratio are obtained and graphically presented in Figure 6. A secondary filter

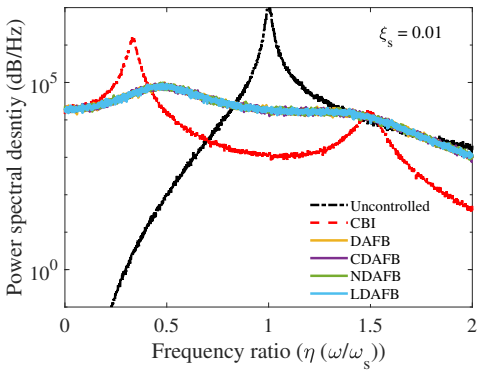

Fig. 6 Variations in the optimal displacements of the single degree of freedom systems isolated by the H_2 optimised ordinary, compound, nested, and levered DAFBs as a function of the frequency ratio of the random white-noise excitation.

using the parameters ω_r and ζ_r yields a constrained power output for ground displacement. Since $\omega_r \ll \omega_d$, the second quotient rapidly approaches unity, therefore the second filter mostly affects the extremely low-frequency range. The filter parameter values are derived from [32] to examine locations with soils categorized as hard, medium, and soft. The medium soil is considered for this study. The maximum dynamic response of the uncontrolled structure is 1.8247×10^7 dB/Hz. The maximum dynamic responses of the structures isolated by CBI, DAFB, CDAFB, NDAFB, and LDAFB have been determined as $1.6{\times}10^6$ dB/Hz, $1.0{\times}10^5$ dB/Hz, 9.54×10^4 dB/Hz, 9.89×10^4 dB/Hz, and 9.31×10^4 dB/Hz. Accordingly, The novel isolators are 93.71 %, 94.03 %, 93.81 %, and 94.17 % superior to the CBI. The resemblance in the frequency response functions (FRFs) and power spectrum densities (PSDs) seen across the four isolator designs is ascribed to the H_2 optimisation method, which guarantees uniform performance under harmonic and white noise stimuli. Although the isolators display varying damping ratios, their optimal characteristics result in similar dynamic responses. This results from the interplay of mass, stiffness, and damping, together with the energy redistribution induced by their amplification processes. The amplifier angles (ϕ, θ, ϕ_1, ϕ_2, ϕ_3) are calibrated to enhance vibration attenuation, addressing variations in damping and structural arrangements. These angles affect the effective damping and stiffness characteristics, allowing all isolators to attain similar dynamic responses. The resultant nonlinear amplification reallocates energy dissipation, resulting in analogous frequency responses across all isolator designs.

The analytical investigations and the simulation works are further validated by a numerical study. Newmark-beta method is employed to conduct the numerical study. This numerical study considers Northridge near-field earthquake data (pulse) as a loading function. The mass of the primary structure is m = 3000 tons. The time interval of the structure is denoted as T = 0.5 seconds. The structural period, $\omega_s = 2\pi/T$, is used to determine the natural frequency of the structure. The predicted viscous damping ratio of the single-degree-of-freedom systems is ξ_s = 0.02. The maximum dynamic response of the uncontrolled structure is 0.0122 m. The maximum dynamic responses of the structures isolated by

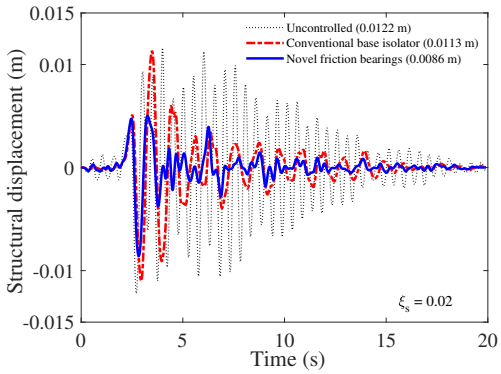

Fig. 7 Variations in the optimal displacements of the single degree of freedom systems isolated by the H_2 optimised ordinary, compound, nested, and levered DAFBs versus the time period of the Northridge earthquake.

CBI and novel friction bearings have been determined as 0.0113 m and 0.0086. Accordingly, The novel friction bearings are 23.80 % superior to the CBI.

4 Summary and conclusions

The paper introduces damping amplifiers integrated into the core material of traditional nonlinear friction base isolators to improve their vibration attenuation efficacy and rectify intrinsic deficiencies. The proposed technology integrates damping amplifiers into the core material via the use of rhombus-type arrangements inside the isolators. These arrangements provide inertial forces that alter the effective damping of the isolators during vibration. The inertial amplification mechanism enhances the damping effect using mechanical configurations, including nested or levered designs, inside the isolator's construction. This integration improves vibration damping by dynamically modifying the isolator's response according to the applied stimulation. Four new types of damping amplifier friction bearings are introduced: LDAFB, NDAFB, CDAFB, and DAFB. The application of the H_2 optimisation technique yields the closed-form analytical solution for the optimum designed parameters. The analytical analysis confirms the efficiency of the newly obtained closed-form equations for the ideal design parameters. The frequency response function was utilised to generate closed-form formulas for the dynamic responses of the isolator and main structure. The harmonic, random white-noise excitation was used as basic excitations. Further, the analytical investigations and the simulation are validated by a numerical study by considering real earthquake load. According to the results, the H_2 optimised DAFB, CDAFB, NDAFB, and LDAFB have vibration reduction capacities that are 76.1 % higher than the optimum conventional base isolator. The experimental activity is the future focus of the research.

ORCID ID

Sudip Chowdhury: https://orcid.org/0000-0001-6218-4843
Sondipon Adhikari: https://orcid.org/0000-0003-4181-3457

Declaration of competing interest

The authors declare that they have no known competing financial interests or personal relationships that could have appeared to influence the work reported in this paper

Acknowledgement

The authors would like to acknowledge the Postdoctoral research grant received from The University of Glasgow for the partial financial support for this research work.

Data Availability Statement

No data, models, or code were generated or used for this paper.

References

[1] Talaeitaba, S. B., Safaie, M., and Zamani, R., 2021, "Development and application of a new base isolation system in low-rise buildings," *Structures*, Vol. 34, Elsevier, pp. 1684–1709.

[2] Dong, W., Shi, Y., Wang, Q., Wang, Y., and Yan, J.-B., 2023, "Development of a long-period vertical base isolation device with variable stiffness for steel frame structures," Soil Dynamics and Earthquake Engineering, **164**, p. 107638.

[3] Jing, W., Feng, J., Wang, S., and Song, S., 2023, "Failure probability of a liquid storage tank with three-dimensional base-isolation under earthquake action," *Structures*, Vol. 58, Elsevier, p. 105633.

[4] Baidya, S. and Roy, B. K., 2023, "Comparative seismic performance of building with Cu-Al-Be and Ni-Ti SMARB base isolation system using particle swarm optimization," Journal of Structural Integrity and Maintenance, **8**(3), pp. 133–139.

[5] Zhang, C., Duan, C., and Sun, L., 2024, "Inter-storey isolation versus base isolation using friction pendulum systems," International Journal of Structural Stability and Dynamics, **24**(02), p. 2450022.

[6] Chen, P., Wang, B., Dai, K., and Li, T., 2022, "Analytical and numerical investigations of base isolation system with negative stiffness devices," Engineering Structures, **268**, p. 114799.

[7] Zhao, C., Zeng, C., Huang, H., Dai, J., Bai, W., Wang, J., and Mo, Y., 2021, "Preliminary study on the periodic base isolation effectiveness and experimental validation," Engineering Structures, **226**, p. 111364.

[8] Nepal, S. and Saitoh, M., 2020, "Improving the performance of conventional base isolation systems by an external variable negative stiffness device under near-fault and long-period ground motions," Earthquake Engineering and Engineering Vibration, **19**, pp. 985–1003.

[9] De Domenico, D., Gandelli, E., and Quaglini, V., 2020, "Effective base isolation combining low-friction curved surface sliders and hysteretic gap dampers," Soil Dynamics and Earthquake Engineering, **130**, p. 105989.

[10] Zhang, C. and Ali, A., 2021, "The advancement of seismic isolation and energy dissipation mechanisms based on friction," Soil Dynamics and Earthquake Engineering, **146**, p. 106746.

[11] Masnata, C., Di Matteo, A., Adam, C., and Pirrotta, A., 2021, "Assessment of the tuned mass damper inerter for seismic response control of base-isolated structures," Structural Control and Health Monitoring, **28**(2), p. e2665.

[12] Islam, N. U. and Jangid, R., 2023, "Optimum parameters and performance of negative stiffness and inerter based dampers for base-isolated structures," Bulletin of Earthquake Engineering, **21**(3), pp. 1411–1438.

[13] Zamani, A.-A. and Etedali, S., 2022, "A new framework of multi-objective BELBIC for seismic control of smart base-isolated structures equipped with MR dampers," Engineering with Computers, **38**(4), pp. 3759–3772.

[14] Chowdhury, S., Banerjee, A., and Adhikari, S., 2024, "Enhancing seismic resilience of nonlinear structures through optimally designed additional mass dampers," International Journal of Non-Linear Mechanics, p. 104717.

[15] Chowdhury, S., Banerjee, A., and Adhikari, S., 2023, "The Exact Closed-Form Expressions for Optimum Inertial Amplifier Coupled Nonlinear Friction Bearing Isolators," *International Conference on Nonlinear Dynamics and Applications*, Springer, pp. 165–176.

[16] Chowdhury, S., Banerjee, A., and Adhikari, S., 2024, "From Impact to Control: Inertially Amplified Friction Bearings," ASCE-ASME Journal of Risk and Uncertainty in Engineering Systems, Part A: Civil Engineering, **10**(4), p. 04024071.

[17] Smith, M. C., 2002, "Synthesis of mechanical networks: the inerter," IEEE Transactions on automatic control, **47**(10), pp. 1648–1662.

[18] Berton, S. and Bolander, J. E., 2005, "Amplification system for supplemental damping devices in seismic applications," Journal of Structural Engineering, **131**(6), pp. 979–983.

[19] Londoño, J. M., Neild, S. A., and Wagg, D. J., 2015, "Using a damper amplification factor to increase energy dissipation in structures," Engineering Structures, **84**, pp. 162–171.

[20] Taniker, S. and Yilmaz, C., 2013, "Phononic gaps induced by inertial amplification in BCC and FCC lattices," Physics Letters A, **377**(31-33), pp. 1930–1936.

[21] Chowdhury, S., Banerjee, A., and Adhikari, S., 2024, "The nonlinear negative stiffness inertial amplifier base isolators for dynamic systems," Mechanics Based Design of Structures and Machines, pp. 1–40.

[22] Chowdhury, S., Banerjee, A., and Adhikari, S., 2024, "The optimal nonlinear inertial amplifier friction bearings for liquid storage tanks: an analytical study," International Journal of Dynamics and Control, pp. 1–12.

[23] Adhikari, S. and Banerjee, A., 2022, "Enhanced low-frequency vibration energy harvesting with inertial amplifiers," Journal of Intelligent Material Systems and Structures, **33**(6), pp. 822–838.

[24] Banerjee, A., Adhikari, S., and Hussein, M. I., 2021, "Inertial amplification band-gap generation by coupling a levered mass with a locally resonant mass," International Journal of Mechanical Sciences, **207**, p. 106630.

[25] Ma, H., Cheng, Z., Shi, Z., and Marzani, A., 2023, "Structural vibration mitigation via an inertial amplification mechanism based absorber," Engineering Structures, **295**, p. 116764.

[26] Yilmaz, C., Hulbert, G. M., and Kikuchi, N., 2007, "Phononic band gaps induced by inertial amplification in periodic media," Physical Review B—Condensed Matter and Materials Physics, **76**(5), p. 054309.

[27] Chowdhury, S., Banerjee, A., and Adhikari, S., 2024, "Enhancing seismic resilience of structures through optimally designed nonlinear negative stiffness base isolators: Exact closed-form expressions," Nonlinear Dynamics, **112**(18), pp. 15833–15856.

[28] Kang, X., Wang, X., Zhang, A., and Xia, G., 2024, "Low Frequency Vibration Energy Harvesting of Piezoelectric Vibration Systems with an Adjustable Device and Inertial Amplifier Device," Journal of Vibration Engineering & Technologies, pp. 1–25.

[29] Zhao, C., Zhang, K., Zhao, P., and Deng, Z., 2023, "Finite-amplitude nonlinear waves in inertial amplification metamaterials: theoretical and numerical analyses," Journal of Sound and Vibration, **560**, p. 117802.

[30] Zhao, Z., Chen, Q., Zhang, R., Pan, C., and Jiang, Y., 2020, "Energy dissipation mechanism of inerter systems," International Journal of Mechanical Sciences, **184**, p. 105845.

[31] Matsagar, V. A. and Jangid, R., 2003, "Seismic response of base-isolated structures during impact with adjacent structures," Engineering Structures, **25**(10), pp. 1311–1323.

[32] Kiureghian, A. D. and Neuenhofer, A., 1992, "Response spectrum method for multi-support seismic excitations," Earthquake engineering & structural dynamics, **21**(8), pp. 713–740.

List of Figures

List of Tables